NANO LETTERS

Letter

pubs.acs.org/NanoLett

Single Ion Channel Recordings with CMOS-Anchored Lipid Membranes

Jacob K. Rosenstein,*[,†,‡] Siddharth Ramakrishnan,[†,§] Jared Roseman,[†] and Kenneth L. Shepard*[,†]

[†]Department of Electrical Engineering, Columbia University, New York, New York 10027, United States

[‡]School of Engineering, Brown University, Providence, Rhode Island 02912, United States

[§]Department of Biology, University of Puget Sound, Tacoma, Washington 98416, United States

Supporting Information

ABSTRACT: We present single-ion-channel recordings performed with biomimetic lipid membranes which are directly attached to the surface of a complementary metal−oxide−semiconductor (CMOS) preamplifier chip. With this system we resolve single-channel currents from several types of bacterial ion channels, including fluctuations of a single alamethicin channel at a bandwidth of 1 MHz which represent the fastest single-ion-channel recordings reported to date. The platform is also used for high-resolution α-hemolysin nanopore recordings. These results illustrate the high signal fidelity, fine temporal resolution, small geometry, and multiplexed integration which can be achieved by leveraging integrated semiconductor platforms for advanced ion channel interfaces.

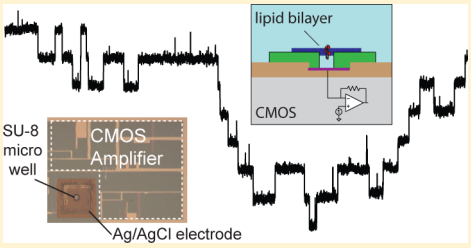

KEYWORDS: *Single-molecule, ion channels, nanopore, CMOS, lipid bilayer, low noise amplifier*

Ion-channel proteins are ubiquitous in the cellular membranes of all living things. Understanding their diverse and central roles in cellular sensing, signaling, and energetics have been important areas of research for many decades,[1] and ion channels remain a major target for drug discovery.[2] Still, the stochastic behavior and delicate structure of ion channels has left challenges in understanding some of the biomolecular mechanisms and dynamics of channel gating, as well as in reliably utilizing isolated ion channels for biotechnology applications, including nanopore DNA sequencing.[3,4]

Ion channels are most often studied using patch-clamp techniques,[5,6] but biophysical studies of some ion channels have employed in vitro planar reconstituted lipid bilayers as model cell membranes. Although comparatively few types of functional proteins have been demonstrated in artificial lipid membranes, reconstituted bilayers are attractive because their chemical makeup can be well-controlled, they involve no live cells, they can be measured outside physiological conditions, and their planar geometry is convenient for electrochemical measurements.[7]

Electronic measurements of ion channels in both patch-clamp and planar bilayer experiments are usually made with voltage-clamp amplifiers, which measure the ionic current as a function of time while applying an electrochemical potential across the membrane through silver/silver-chloride (Ag/AgCl) electrodes. Ionic conductance varies between types of ion channels, but their nanoscale dimensions typically produce single-channel currents on the order of picoamperes or femtoamperes. These weak signals confront the noise floor of available electronic amplifiers, and single-channel recordings are generally constrained in both amplitude and temporal resolution by low signal-to-noise ratios.[6] Current noise amplitudes invariably increase for wider measurement bandwidths while the signal amplitude is unchanged, resulting in a signal-to-noise ratio which decreases as temporal resolution is improved.

While the low-frequency noise of ion channel measurements is often dominated by the noise of the channel itself, the high-frequency noise is limited by the measurement electronics and is a strong function of experimental capacitances (see Supplementary Discussion). The voltage-clamp amplifier's equivalent input voltage noise v_n (V Hz$^{-1/2}$) produces noise currents through all capacitances at the amplifier input ($\sum C$), with a root-mean-squared amplitude given by:

$$I_{\mathrm{RMS}} = \frac{2\pi}{\sqrt{3}} B^{3/2} v_n \sum C$$

where B is the measurement bandwidth. The most commonly described capacitance in lipid bilayer experiments is that of the lipid membrane itself (C_M); lipid bilayers are very thin and exhibit a specific capacitance on the order of 0.5 μF/cm^2. Circular planar bilayers with diameters ranging from 1 to 200 μm, therefore, have C_M ranging from 4 fF to 150 pF. For larger bilayers, C_M can be the single dominant parasitic in the system, and reductions to the bilayer area translate directly to lower measurement noise.[8] For smaller bilayers, however, other parasitics are equally important, in particular the input capacitance (C_I) of the voltage-clamp amplifier and wiring capacitance (C_W) from connections between the electrodes and

Received: March 5, 2013
Revised: April 17, 2013

   dx.doi.org/10.1021/nl400822r | *Nano Lett.* XXXX, XXX, XXX−XXX

the amplifier. With popular electrophysiology amplifiers (such as the Axopatch 200B or HEKA EPC-10), C_I is on the order of 10−20 pF, limiting the noise benefits that would be seen from reducing the bilayer diameter below 30 μm. Yet methods to produce smaller bilayers exist,[8−11] and if paired with amplifiers with appropriately reduced input capacitance, these bilayer area reductions can continue to yield noise reductions.

In the literature there are several examples of patch-clamp studies using aftermarket modifications of an Axopatch 200B amplifier.[12,13] These customizations yielded lower noise floors and higher signal bandwidths, with the fastest previously reported single-channel data reaching a bandwidth of 250 kHz with corresponding noise of 12.7 pA_{RMS}.[13] There are also several examples of integrated current preamplifiers for ion channel recordings,[14−17] an approach which offers the flexibility to reduce C_I below what is practical with discrete transistors.

We previously demonstrated a voltage-clamp preamplifier integrated circuit (IC) in a commercial 130 nm CMOS process, in which each amplifier occupies just 0.4 mm^2 and has C_I = 1 pF. Very low parasitic capacitances allowed us to resolve ionic current signals through solid-state nanopores at a bandwidth of 1 MHz,[17] more than 10 times faster than can be recorded by commercially available instruments. In this Letter, we apply this platform to similarly reduce parasitic capacitances in biological ion channel recordings, by direct attachment of a lipid bilayer to the surface of the IC. This arrangement enables noise-limited bandwidths in excess of 1 MHz to be achieved on an integrated platform which will ultimately be scalable to the independent recording of thousands of channels.

Starting with the custom CMOS amplifier chip,[17] we chemically remove the standard aluminum metallization from the amplifier input pads, followed by vacuum deposition of 5 nm Ti and 200 nm Ag and patterning of 20 μm or 30 μm diameter microwells in 5-μm-thick SU-8 (see Supplementary Discussion). A micrograph of the final structure for a single amplifier channel is shown in Figure 1b. After wirebonding and

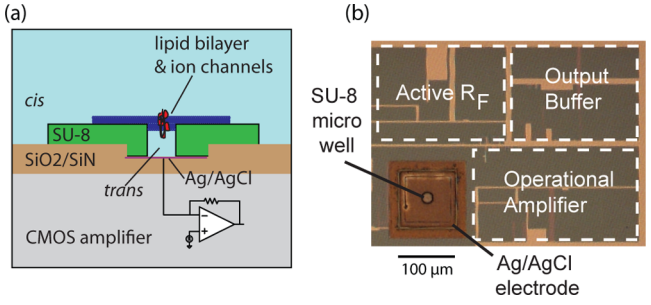

Figure 1. CMOS-anchored lipid membranes. a, Illustrated cross-section of a lipid bilayer formed over an SU-8 microwell on the surface of the CMOS amplifier die. b, Micrograph of one amplifier channel postprocessed with a thin-film silver electrode and SU-8 microwell.

epoxy encapsulation, a 1 mL fluid chamber is assembled around the amplifier chip. With the amplifier mounted on a circuit board, we fill the fluid chamber with electrolyte and chlorinate the silver microelectrode. We then apply ∼0.5 μL of DPhPC solution (10 mg/mL diphytanoyl phosphatidylcholine in *n*-decane) over the SU-8 surface using an air bubble at the tip of micropipet. The lipids spontaneously form bilayers spanning the surface of the microwells, as illustrated in the cross-section of Figure 1a.

These lipid-sealed microwells are similar to lipid bilayer arrays which were previously demonstrated on passive glass substrates[10,18] The one-sided geometry of these microwells means that after each is covered by a lipid membrane, it is electrically isolated; multiple wells can be addressed in parallel, with independent *trans* Ag/AgCl electrodes and one shared *cis* reservoir.

A common concern with microscale Ag/AgCl electrodes is their depletion over time; the mass of available silver determines the net charge ($Q = I_{DC} \times t$) which can be measured over the lifetime of the sensor.[19] Due to the lower DC currents required for ion channels as compared to prior demonstrations with solid-state nanopores, we elected to use a thin evaporated silver film rather than a thicker electroplated layer. The entire 100 μm × 100 μm × 200 nm electrode contains approximately 21 ng of silver, which, when fully converted to AgCl, corresponds to a charge transfer of 19 μC. This places an upper bound on the electrode lifetime of ∼2 days at 100 pA bias. (Much of the electrode is covered by SU-8, but at least some the covered silver is likely still electrochemically available.[20]) The small volume of the *trans* chamber (∼1.6 pL) helps to limit dissolution of the AgCl; although AgCl is highly soluble in water ($K_{SP} = 1.8 \times 10^{-10}$), 2 pL of water becomes saturated with AgCl after dissolving just femtograms of AgCl. During testing, we found that each electrode commonly lasted for several hours.

Knowing the geometry of the amplifier and bilayer support, we can build a simple electrical model for the expected measurement capacitances (Figure 2a). A DPhPC bilayer with a

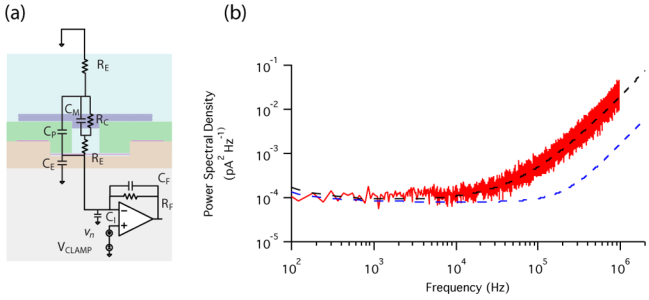

Figure 2. Circuit model and noise spectral density. a, Equivalent circuit model of the lipid bilayer and current preamplifier, including the electrode resistance (R_E), channel resistance (R_C), feedback resistance (R_F), membrane capacitance (C_M), electrode capacitance (C_E), passivation capacitance (C_P), amplifier input capacitance (C_I), and feedback capacitance (C_F). b, The measured input-referred noise power spectral density (A^2 Hz^{1-}) is shown for a dry open-headstage condition (polynomial fit, blue dashed line) and with a DPhPC lipid bilayer formed over a 20-μm-diameter microwell (measured, red; polynomial fit, black dashed line). The total capacitance $\sum C = (C_I + C_F + C_M + C_E + C_P)$ is approximately 3 pF.

nominal diameter of 20 μm has a capacitance C_M = 1.4 pF. The "wiring" capacitance in this case consists of the capacitance between the 100 μm electrode and the silicon substrate (C_E) plus the capacitance between the SU-8 passivated portion of the electrode and the electrolyte (C_P), collectively contributing 120 fF. Summed together with C_I = 1 pF and C_F = 0.15 pF, these add up to an expected total of $\sum C = (C_I + C_F + C_M + C_E + C_P) \approx 3$ pF.

Figure 2b shows the measured input-referred noise power spectral density for an amplifier channel with no input, as well as with a lipid membrane. In both cases, below 10 kHz the

dx.doi.org/10.1021/nl400822r | *Nano Lett.* XXXX, XXX, XXX−XXX

noise is determined by the white noise of the amplifier feedback network. With the bilayer present, at higher frequencies the noise density is fit by $S_n(f) \approx (2\pi f \times 3\ \mathrm{pF} \times 5\ \mathrm{nV\ Hz^{-1/2}})^2$, consistent with the estimate above. The time-domain current noise is evaluated from the integral of the noise spectrum up to a given bandwidth. If a fourth-order low-pass Bessel filter is applied at various cutoff frequencies (f_c), this integrated baseline noise current in the presence of the bilayer corresponds to 1 pA_{RMS} for f_c = 10 kHz, 4.4 pA_{RMS} at 100 kHz, 11.8 pA_{RMS} at 250 kHz, and 61 pA_{RMS} at 1 MHz.

Since the amplifier was originally designed to support DC bias currents as large as 15 nA while operating from a 1.5 V power supply, it uses an active feedback network whose white noise contribution ($\sim$ 10 fA $Hz^{-1/2}$) determines the low-frequency noise floor of the system. Phenomena which require noise amplitudes below 1 pA_{RMS} may be better served by higher-gain preamplifiers with a smaller dynamic range, but for the many applications in which 1 pA_{RMS} or more is acceptable, reduced high-frequency noise density provides an opportunity to acquire meaningful data at much finer temporal resolution. This is a common trade-off associated with integrated microelectronics; low-frequency noise reductions can be more challenging because of difficulties integrating high-value resistors and low-noise devices such as junction field-effect transistors, while high-frequency noise is naturally lower due to reduced capacitive parasitics.

To verify the bilayer structure of our CMOS-anchored lipid membranes, we perform measurements of gramicidin, an antibiotic peptide which increases the permeability of cell membranes.[21−24] Gramicidin produces transient dimer channels in lipid bilayers, formed by junctions between peptides in opposing halves of the membrane. Gramicidin ion channels form and dissociate stochastically irrespective of applied voltage, yielding stepwise current changes in voltage-clamp recordings. Prior to forming a bilayer, < 0.5 μL of gramicidin solution (1 μg/mL in ethanol) is added to the electrolyte such that it is present in both the *cis* and the *trans* chambers. Shortly after painting the lipids, random stepwise current fluctuations are observed. An example recording of gramicidin is shown in Figure 3, showing several simultaneously active channels producing discrete current levels separated by approximately 4 pA.

To explore biotechnology applications of this integrated platform, we consider α-hemolysin (α-HL), a well-studied bacterial toxin which forms heptameric ion channels in cell membranes.[25] In recent years, α-HL has attracted considerable interest as a nanopore sensor with the potential to enable high-speed DNA sequencing, among other applications.[4,26] The channel of an α-HL pore has a diameter of approximately 1.4 nm at its smallest constriction, and the presence of even very small molecules within a single channel can measurably modulate its ionic conductance.

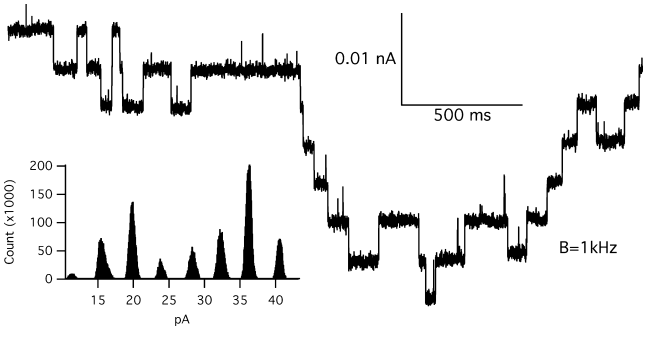

Figure 3. Single gramicidin channels. Recordings of single gramicidin channels in the amplifier-attached lipid bilayers. This trace was measured in 1 M KCl at 100 mV bias and digitally filtered to 1 kHz bandwidth. Inset: An all-points histogram showing the discrete current levels.

Figure 4 shows a current trace measured with a single α-HL nanopore inserted into a lipid bilayer on the CMOS chip in the presence of polydisperse polyethylene glycol (PEG, average m.w. 1500). At 50 mV bias in 4 M KCl, the steady-state current through the pore is 200 pA, and intermittent blockage events decrease this current to approximately 25% of its open value. Each blockade corresponds a single PEG molecule temporarily occupying the pore.[18,27,28] The residual current during each of these events is remarkably stable, and even at a signal bandwidth of 250 kHz, the event edge rates are limited by the filter characteristics rather than the experimental system.

A range of PEG polymer lengths are present in the solution, and each size molecule modulates the α-HL conductance by a different degree. Tabulating the mean residual current level during each event yields a histogram with discrete levels corresponding to the distinct PEG polymer lengths.[28] Figure 4e shows a histogram of the depths of 7642 events recorded over the course of six minutes. The histogram shows distinct peaks separated by approximately 2 pA and each having a standard deviation of $\sim$0.5 pA. The appearance of discrete peaks demonstrates the stability of the amplifier, electrodes, bilayer, and α-HL channel over the length of this data set. Since each point in the histogram is the average of all points in an event, each point has an expected amplitude error roughly corresponding to the integrated current noise from DC to $1/(2\tau)$ Hz, where τ is the duration of the events. By restricting the data set to events longer than 0.5 ms, the peaks have a standard deviation of 10 $[\mathrm{fA/(Hz^{1/2})}] \times [1/(2 \times 0.5\ \mathrm{ms})]^{1/2} \approx 0.5$ pA. This is a marginally higher variance than has been measured with discrete amplifiers,[18,28] which is a result of prioritizing a large dynamic range during the design of the integrated amplifier, as discussed earlier.

Another common reconstituted ion channel is alamethicin, which presents a large conductance and thus can tolerate the increased noise levels which accompany higher bandwidths. Alamethicin is a 20-amino-acid peptide that assembles into small homomeric clusters in lipid bilayers.[29,30] These peptide groups can form voltage-gated ion channels with discrete conductance levels that correspond to integer numbers of participating alamethicin molecules. The conductance levels have a quadratic dependence on the level number and appear as characteristic staircase current patterns in voltage-clamp recordings.[29,31]

Figure 5 shows a recording of alamethicin channels in the CMOS-attached lipid bilayers. After forming lipid bilayers on the amplifier chip, 1 μL of 10 μg/mL alamethicin in ethanol is added to the *cis* chamber. Shortly after adding the peptides, channel current bursts appeared at negative bias voltages.

In other lipid bilayer platforms[8,10,32] it has been shown that alamethicin gating transitions occur faster than can be resolved by commercial patch-clamp amplifiers. Here, we take advantage of higher signal bandwidth to closely examine these conductance transitions. Figure 6 shows expanded images of the rising and falling transitions from the channel burst in Figure 5d, at both 50 kHz and 1 MHz signal bandwidth. At 50 kHz, we observe that the transition edges are limited by the rise

dx.doi.org/10.1021/nl400822r | Nano Lett. XXXX, XXX, XXX−XXX

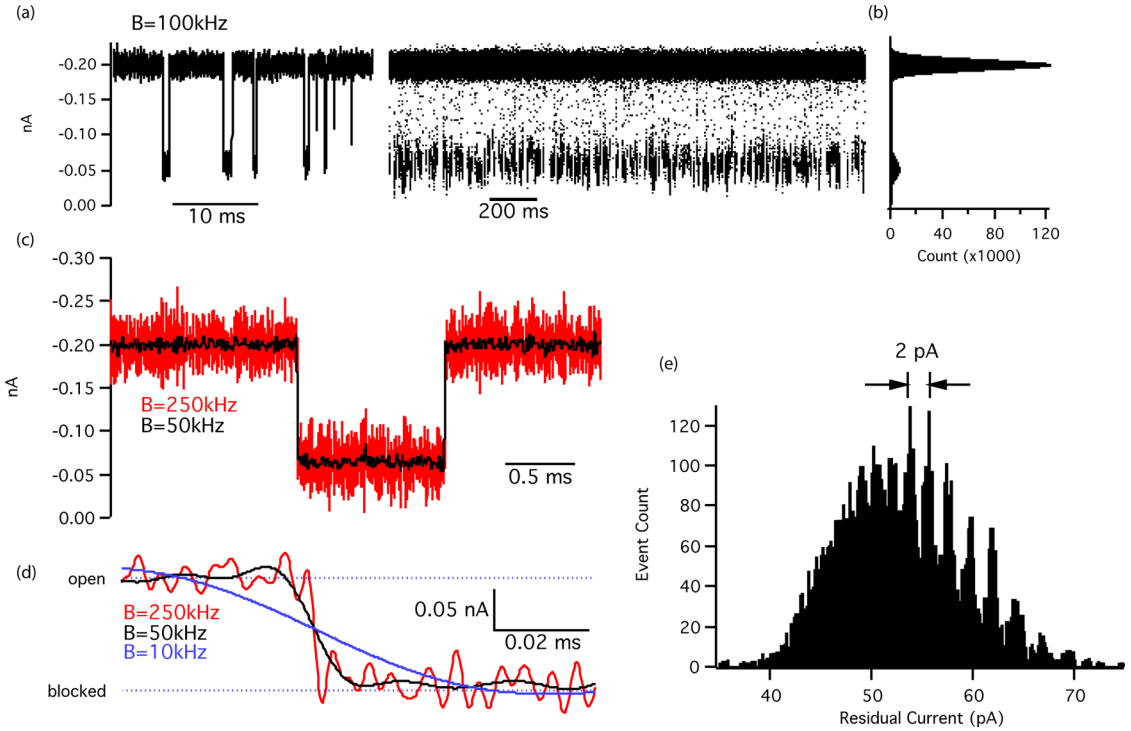

Figure 4. Nanopore mass spectrometry. a, A single α-hemolysin channel in the presence of polydisperse polyethylene glycol (PEG, average m.w. 1500). Each rectangular current blockade corresponds to a single PEG molecule occupying the channel. The trace is shown at B = 100 kHz. b, All-points histogram of the trace, showing clear separation between open and blocked current levels. c, One of the PEG events, digitally filtered to 50 kHz and 250 kHz bandwidths. d, Magnified view of the falling edge of the event, contrasting the signal fall-time at 10 kHz, 50 kHz, and 250 kHz bandwidths. e, Histogram of the average residual current in 7642 events with durations of at least 0.5 ms. Each peak in the histogram corresponds to a unique PEG polymer length.

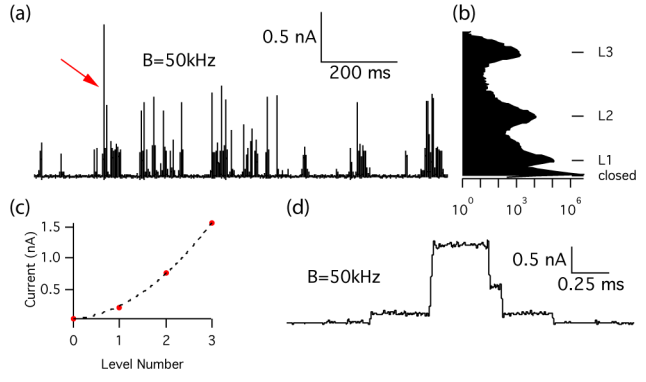

Figure 5. Single alamethicin channels. a, Recordings of single alamethicin channel bursts in 3 M KCl at 150 mV bias, digitally filtered to 50 kHz bandwidth. b, All-points histogram of the trace, showing three distinct conductance levels. c, The discrete current levels identified in the histogram have a quadratic dependence on the level number. d, A magnified view of one of the channel bursts, identified by the red arrow.

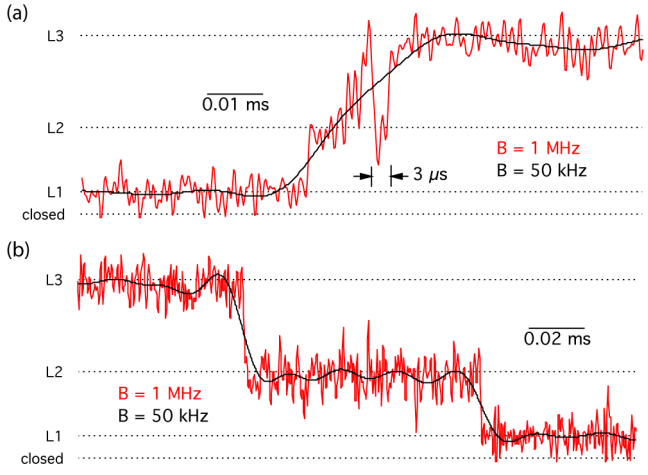

Figure 6. Fast ion channel gating. a, Rising edge of the alamethicin channel burst shown in Figure 5d, sampled at 4 MS/s and digitally filtered to 50 kHz and 1 MHz bandwidths. At 1 MHz it is evident that transition between L1 and L3 includes two stays at L2, lasting 6 and 3 μs, respectively. b, Falling edge of the same channel burst. The closing transitions are briefer than can be resolved in our measurements, even at 1 MHz bandwidth, suggesting that the channel's actual ionic conductance changes in less than 500 ns.

time of the low-pass filter ($\sim$ 10 μs), and as a result short-lived conductance levels briefer than $\sim$20 μs are not captured. In the same trace at 1 MHz, the transition times are indeed much faster than 10 μs. Flickering conductance levels as brief as 3 μs are evident during some channel openings, while during the channel closures the steps usually appear sharp even at this higher bandwidth; thus, we can infer that these transitions occur in less than 500 ns. To the best of our knowledge, these measurements represent the fastest single ion channel recordings achieved to date.

In this Letter we have shown that an active CMOS amplifier chip can simultaneously serve as the physical support and electronic interface for microscale lipid bilayers,[7] creating a powerful platform for high-throughput biotechnology applications such as DNA sequencing and drug discovery. Scaling the sensor and electronic signal chain to submillimeter dimensions

dx.doi.org/10.1021/nl400822r | *Nano Lett.* XXXX, XXX, XXX−XXX

decreases parasitic capacitances and enables measurements of ion channel gating transitions faster than 1 μs. In addition to the parallelism that will be enabled by integrating ion channels with microelectronics, these newly accessible time scales overlap with the durations of molecular dynamics simulations,[33] making it conceivable that soon it will be possible to directly correlate kinetic processes within simulations and measurements of single-molecule ion channel gating.

■ ASSOCIATED CONTENT

Supporting Information

Experimental methods and electronic circuit description. This material is available free of charge via the Internet at http://pubs.acs.org.

■ AUTHOR INFORMATION

Corresponding Author

*E-mail: Jacob_Rosenstein@brown.edu or shepard@ee.columbia.edu.

Notes

The authors declare no competing financial interest.

■ ACKNOWLEDGMENTS

The authors thank Daniel Fleischer for his assistance. This work was supported by the National Institutes of Health under Grant R01-HG006879.

■ REFERENCES

(1) Hille, B. *Ion Channels of Excitable Membranes*, 3rd ed.; Sinauer Associates: Sunderland, MA, 2001.

(2) Wood, C.; Williams, C.; Waldron, G. J. *Drug Discovery Today* **2004**, *9*, 434−41.

(3) Branton, D.; Deamer, D. W.; Marziali, A.; Bayley, H.; Benner, S. A.; Butler, T.; Di Ventra, M.; Garaj, S.; Hibbs, A.; Huang, X.; Jovanovich, S. B.; Krstic, P. S.; Lindsay, S.; Ling, X. S.; Mastrangelo, C. H.; Meller, A.; Oliver, J. S.; Pershin, Y. V.; Ramsey, J. M.; Riehn, R.; Soni, G. V.; Tabard-Cossa, V.; Wanunu, M.; Wiggin, M.; Schloss, J. A. *Nat. Biotechnol.* **2008**, *26*, 1146−53.

(4) Bayley, H.; Cremer, P. S. *Nature* **2001**, *413*, 226−30.

(5) Hamill, O. P.; Marty, A.; Neher, E.; Sakmann, B.; Sigworth, F. J. *Pflugers Arch.* **1981**, *391*, 85−100.

(6) Sakmann, B.; Neher, E. *Single-Channel Recording*; Springer: New York, 2009.

(7) Zagnoni, M. *Lab Chip* **2012**, *12*, 1026−39.

(8) Mayer, M.; Kriebel, J. K.; Tosteson, M. T.; Whitesides, G. M. *Biophys. J.* **2003**, *85*, 2684−95.

(9) Fertig, N.; Meyer, C.; Blick, R.; Trautmann, C.; Behrends, J. *Phys. Rev. E* **2001**, *64*, 1−4.

(10) Baaken, G.; Sondermann, M.; Schlemmer, C.; Rühe, J.; Behrends, J. C. *Lab Chip* **2008**, *8*, 938−44.

(11) White, R. J.; Ervin, E. N.; Yang, T.; Chen, X.; Daniel, S.; Cremer, P. S.; White, H. S. *J. Am. Chem. Soc.* **2007**, *129*, 11766−75.

(12) Parzefall, F.; Wilhelm, R.; Heckmann, M.; Dudel, J. *J. Physiol.* **1998**, 181−188.

(13) Shapovalov, G.; Lester, H. A. *J. Gen. Physiol.* **2004**, *124*, 151−61.

(14) Kim, D.; Goldstein, B.; Tang, W.; Sigworth, F. J.; Culurciello, E. *IEEE Trans. Biomed. Circuits Syst.* **2012**, 1−11.

(15) Goldstein, B.; Kim, D.; Xu, J.; Vanderlick, T. K.; Culurciello, E. *IEEE Trans. Biomed. Circuits Syst.* **2012**, *6*, 111−119.

(16) Kim, J.; Maitra, R.; Pedrotti, K.; Dunbar, W. *IEEE Trans. Biomed. Circuits Syst.* **2012**, 1−1.

(17) Rosenstein, J. K.; Wanunu, M.; Merchant, C. A.; Drndic, M.; Shepard, K. L. *Nat. Methods* **2012**, 9.

(18) Baaken, G.; Ankri, N.; Schuler, A.-K.; Rühe, J.; Behrends, J. C. *ACS Nano* **2011**, *5*, 8080−88.

(19) Polk, B. J.; Stelzenmuller, A.; Mijares, G.; MacCrehan, W.; Gaitan, M. *Sens. Actuators B* **2006**, *114*, 239−247.

(20) Suzuki, H.; Hiratsuka, A.; Sasaki, S.; Karube, I. *Sens. Actuators* **1998**, *46*, 104−113.

(21) Hladsky, S. B.; Haydon, D. A. *Biochim. Biophys. Acta* **1972**, *274*, 294−312.

(22) Bamberg, E.; Noda, K.; Gross, E.; Lauger, P. *Biochim. Biophys.Acta* **1976**, *419*, 223−228.

(23) Kelkar, D. A.; Chattopadhyay, A. *Biochim. Biophys. Acta* **2007**, *1768*, 2011−25.

(24) Andersen, O. S. *Biophys. J.* **1983**, *41*, 119−33.

(25) Bhakdi, S.; Tranum-Jensen, J. *Microbiol. Rev.* **1991**, 55.

(26) Kasianowicz, J. J.; Brandin, E.; Branton, D.; Deamer, D. W. *Proc. Natl. Acad. Sci. U.S.A.* **1996**, *93*, 13770−3.

(27) Reiner, J. E.; Kasianowicz, J. J.; Nablo, B. J.; Robertson, J. W. F. *Proc. Natl. Acad. Sci. U.S.A.* **2010**, *107*, 6−11.

(28) Robertson, J. W. F.; Rodrigues, C. G.; Stanford, V. M.; Rubinson, K. A.; Krasilnikov, O. V.; Kasianowicz, J. J. *Proc. Natl. Acad. Sci. U.S.A.* **2007**, *104*, 8207−11.

(29) Cafiso, D. S. *Annu. Rev. Biophys. Biomol. Struct.* **1994**, *23*, 141−65.

(30) Ramakrishnan, N.; Balaram, P. *Acc. Chem. Res.* **1981**, 356−362.

(31) Gordon, L. G.; Haydon, D. A. *Philos. Trans. R. Soc. London, Ser. Bs* **1975**, *270*, 433−47.

(32) Sondermann, M.; George, M.; Fertig, N.; Behrends, J. C. *Biochim. Biophys. Acta* **2006**, *1758*, 545−51.

(33) Klepeis, J. L.; Lindorff-Larsen, K.; Dror, R. O.; Shaw, D. E. *Curr. Opin. Struct. Biol.* **2009**, *19*, 120−7.